Transcription factor FOXM1 specifies the loading of chromatin DNA to extracellular vesicles

Yunsheng Zhang[1,2], Nana Ding[1], Yizhen Li[1], Xiaoyun Zhao[1], Shiping Yang[1], Ping Fu[1], Yousong Peng[1], Haojie Cheng[1], Min Ouyang[1], Ruiping Wang[1], Yu Wang[1], Hanyun Liu[1], Yan Chen[1], Xiaoqin Huang[1], Li Yu[1], and Yongjun Tan[1*]

[1] State Key Laboratory of Chemo/Biosensing and Chemometrics, College of Biology, Hunan Engineering Research Center for Anticancer Targeted Protein Pharmaceuticals, Hunan University, Changsha, Hunan 410082, PR China.

[2] The Second Affiliated Hospital, University of South China, Hengyang, Hunan 421001, PR China.

**** Correspondence to:*** Dr. Yongjun Tan, E-mail: yjtan@hnu.edu.cn

Abstract

Extracellular vesicle DNA (evDNA) acts as a potential mechanism for intercellular communication and possesses an important diagnostic value for multiple diseases. In this study, we have provided the first example that transcription factor determines the sources of evDNA from chromatin DNA. Transcription factor FOXM1 mediates the loading of specific chromatin DNA fragments into extracellular vesicles (EVs). Specifically, certain chromatin DNA fragments are specified by FOXM1 and form LC3-FOXM1-DNA vesicles in cytoplasm. Then the cytoplasmic LC3-FOXM1-DNAs are transported to EVs through the process of an autophagosome-MVB transport. The roles of FOXM1 on loading the DNA fragments to cytoplasm and then EVs are further supported by the results of the DNA-FISH experiment, the visualization of TetR-GFP on the DNA fragments from the certain chromatin loci with a knock-in TetO array, and the transfection of a constructed DNA containing multiple FOXM1 binding sites into cells followed by the measurements of the DNA in EVs. We have proved that the LC3-FOXM1-DNAs exist on outside the lumen of EVs as a linear DNA form. Furthermore, the LC3-FOXM1-DNAs of EVs can be absorbed by recipient cells and stay in the recipient cells as long as four weeks. This discovery provides a new clue to understand the sources of evDNA and to further study the potential functions of evDNA in the future.

Key words

Extracellular vesicle DNA; Transcription factor; FOXM1; Extracellular vesicles

Extracellular vesicle DNA (evDNA) carries portions of parent cells' genetic information about the physiological or pathological processes and is considered to act as an intercellular messenger or to maintain cellular homeostasis[1,2]. Although extensive studies have declared its diagnostic value of diseases, the mechanism of DNA loading in extracellular vehicles (EVs) remains elusive and the potential fate or function of evDNA is rarely discussed. Here we show that a transcription factor-involved machinery specifies certain chromatin DNA fragments to EVs and consequently the released evDNA can be absorbed by recipient cells. The tested evDNA can stay in the recipient cells for a long period, providing a clue to explain how a cell releases its evDNA to affect other cells. Forkhead Box M1 (FOXM1), a typical proliferation-associated transcription factor[3], can mediate the loading of specific chromatin DNA fragments to EVs through interacting with LC3 protein. LC3, also called MAP1LC3B or LC3B, is a key member of Atg8 protein family regulating autophagy[4] and has been found to locate in nucleus and associate with chromatin[5]. LC3 is found to specify the loading of proteins and RNAs to EVs[6]. However, whether nuclear LC3 mediates the secretion of chromatin DNA is not well known. We show that certain chromatin DNA fragments, FOXM1, and LC3 together can form vesicles in cytoplasm and eventually are released by EVs. The FOXM1-LC3 interaction is required for chromatin DNA transporting to EVs because inhibiting FOXM1-LC3 interaction diminishes the evDNA loading. Our study suggests that transcription factor FOXM1 can determine the sources of evDNA from chromatin DNA, providing an example of evDNA biogenesis to explain its sources and potential fate or function.

The formation of LC3-FOXM1-DNA vesicles in cytoplasm

First, we observed that LC3-FOXM1-DNA vesicles formed in cytoplasm of human lung carcinoma epithelial A549 cells (**Fig. 1a**). The phenomena were also observed in other human cells such as breast

cancer MDA-MB-231 and MCF-7 cells, and human embryonal kidney HEK293T cells (**Extended Data Fig. 1a, b**). Furthermore, we observed that starvation increased the accumulation of double-stranded DNA in cytoplasm, which were correlated with the appearance of LC3-FOXM1-DNA vesicles (**Fig. 1b**). The LC3-FOXM1-DNA vesicles could be enhanced by different stress conditions such as starvation, rapamycin, H_2O_2, or DNA damage reagent etopside (**Extended Data Fig. 1c**). After introduced into cells, the exogenous RFP-FOXM1 and GFP-LC3 proteins co-localized in the chromatin DNA-containing cytoplasmic vesicles (**Extended Data Fig. 1d, e**). The RFP-FOXM1 ΔDBD proteins, in which FOXM1-DNA binding domain (DBD)[7] was deleted, could not appear in the chromatin DNA-containing cytoplasmic vesicles (**Extended Data Fig. 1f**), implicating that the FOXM1 DNA-binding abilities were required for the formation of LC3-FOXM1-DNA vesicles in cytoplasm.

We performed chromatin immunoprecipitation sequencing (ChIP-seq) analysis to obtain FOXM1-associated chromatin DNA sequences (named as M1-ADs), LC3-associated chromatin DNA sequences (named as LC3-ADs), and then identify multiple overlaps (named as LC3-M1-ADs, n=100) between M1-ADs and LC3-ADs (**Fig. 1c, d and Extended Data Fig. 2a, Table S1**). We chose three LC3-M1-ADs (LC3-M1-AD1, LC3-M1-AD2, and LC3-M1-AD3) as examples to perform FOXM1 or LC3 ChIP-qPCR and confirmed the association between these chromatin loci and FOXM1 or LC3 (**Fig. 1e and Extended Data Fig. 2b, c**). The DNA-pulldown assays further confirmed that LC3-M1-AD1 could bind to FOXM1 and LC3 proteins (**Extended Data Fig. 3a**). Again, the electrophoretic mobility shift assays (EMSA) demonstrated that FOXM1, LC3, and LC3-M1-AD1 could form an LC3-FOXM1-DNA complex (**Extended Data Fig. 3b**). We performed DNA-FISH experiments to show the existence of LC3-M1-AD1 in cytoplasm (**Fig. 1f and Extended Data Fig. 3c**). Furthermore, we knocked in a TetO array (96x), which can be visualized by exogenously expressed TetR-GFP[8], at

the locus of LC3-M1-AD3 by CRISPR/cas9 in A549 cells **(Extended Data Fig. 3d)**, and also observed the existence of LC3-M1-AD3 in cytoplasm **(Fig. 1g)**. Cytoplasmic DNA was extracted particularly[9] and the levels of LC3-M1-ADs or TetO-knockin fragments in cytoplasm were elevated by starvation (**Extended Data Fig. 3e, f**). Together, these data suggested that transcription factor FOXM1 could specify the loading of certain chromatin DNA fragments into cytoplasmic LC3-FOXM1-DNA vesicles.

The interaction between FOXM1 and LC3

The co-localization of FOXM1 and LC3 was also observed in nucleus to help the calculation of Pearson Correlation Coefficient value (0.66 ± 0.08) (**Fig. 2a**). The co-immunoprecipitation (co-IP) experiments revealed that FOXM1 interacted with the lipidated LC3-II[10] in cells (**Fig. 2b and Extended Data Fig. 4a**). A bimolecular fluorescence complementation (BiFC) assay[11] confirmed that the FOXM1-LC3 interaction appeared mainly in nucleus (**Fig. 2c**) and relied on the LC3 lipidation, evidenced by that the G120A-mutated LC3 (the lipidation-deficient mutant[5]) was not able to interact with FOXM1 (**Extended Data Fig. 4b**). The FOXM1-LC3 interaction was further confirmed by the co-IP with exogenous Flag-FOXM1 and GFP-LC3 proteins (**Extended Data Fig. 5a**) or by glutathione *S*-transferase (GST)-pulldown assays with recombinant GST-LC3 proteins (**Extended Data Fig. 5b**). The results of co-IP with the exogenous Flag-FOXM1 and the G120A-mutated GFP-LC3 showed again that the deficiency of LC3 lipidation impaired the FOXM1-LC3 interaction (**Extended Data Fig. 6**).

We mapped the critical regions mediating the FOXM1-LC3 interaction on FOXM1 and LC3 proteins and first found that the DNA-binding domain of FOXM1 (FOXM1-DBD) was required for LC3 binding to FOXM1 (**Fig. 2d and Extended Data Fig. 7a**) and FOXM1-DBD alone could interact with LC3 in GST-LC3-pulldown assays (**Fig. 2e**). We further found that FOXM1-DBD interacted with lipidated LC3-II (**Extended Data Fig. 7b**). The overexpression of GFP-FOXM1-DBD abolished the

endogenous FOXM1-LC3 interaction and impaired FOXM1-DNA vesiculation in cytoplasm (**Extended Data Fig. 7c and d**). It is known that so-called LC3-interacting region (LIR) motif exists in LC3' substrate proteins[12,13]. We analyzed the protein sequence of FOXM1-DBD and identified four LIR motifs (263-266, 273-276, 307-310 and 317-320), which were evolutionarily conserved among FOXM1s of human, mouse, rat, and macaque (**Extended Data Fig. 8a**). We generated four FOXM1-DBD mutants (Y263A, F273A, F307A and Y317A, corresponding to the four LIR motifs respectively) and determined that the LIR motif (317-320) in FOXM1-DBD was necessary for LC3 binding to FOXM1 (**Fig. 2f**). Rosetta Flex ddG[14] alanine-scanning analysis was performed with the amino acid sequence of the LIR motif (317-320) and LC3 protein structure[15], and predicted that the Y317A mutation significantly elevated the free energy of binding and consequently disrupted the interaction between this LIR motif and LC3 (**Extended Data Fig. 8b**).

The residues R10, R11, and F52 of LC3 have been identified to contribute for the interaction of LC3 with other proteins[5,16]. We identified that the aa29-128 region (containing F52) of LC3 was required for the FOXM1-LC3 interaction but not the aa1-28 region (containing R10 and R11) of LC3 (**Fig. 2g**). Rosetta Dock[17] was performed with the known structures of FOXM1-DBD[18] and LC3 to simulate the FOXM1-LC3 interaction and predicted the formation of potential hydrogen bonds between the LIR motif (317-320) of FOXM1 and the residue F52 of LC3 (**Fig. 2h**). Thus, we generated an LC3 F52A mutant and found that this mutant could not interact with FOXM1, similar as the LC3 G120A mutant (see above) (**Fig. 2i**).

The transport of LC3-FOXM1-DNAs to cytoplasmic MVBs

We were able to detect the cytoplasmic translocation of endogenous FOXM1 during starvation or rapamycin treatment (**Extended Data Fig. 9a-c**), same as the exogenously expressed FOXM1

(**Extended Data Fig. 10a-c and Movie 1**). The lipidated LC3-II, as an autophagosomal marker[10], could be detected as dots in cytoplasm (**Extended Data Fig. 11a and b**). As expected, we found that the co-localized dots of FOXM1 and LC3 in cytoplasm were dramatically increased during starvation (**Extended Data Fig. 12a and b**). Atg5 is a key regulator essential for LC3 lipidation[19] and we found that the knockout of Atg5 inhibited the cytoplasmic translocation of FOXM1 in Atg5$^{-/-}$ cells (**Extended Data Fig. 12c**). Furthermore, the analysis of cytoplasmic DNA from FOXM1$^{-/-}$ cells or Atg5$^{-/-}$ cells showed a decrease in levels of LC3-M1-ADs (**Fig. 3a and b**), suggesting that a FOXM1 and lipidated LC3-II-involved mechanism mediated the translocation of LC3-M1-ADs into cytoplasmic autophagosomes.

Although autophagosomes mediate the degradation of cellular components by fusing with endosomes/lysosomes[20,21], accumulating evidences prove that the endosomes undergo fusion and fission events to mature into multivesicular bodies (MVBs, a special kind of late endosomes[22]) for the secretion of cellular cargos[6,23,24]. Moreover, MVBs contain subpopulations of LC3-positive intraluminal vesicles (ILVs)[6]. To confirm the existence of FOXM1 in MVBs, we performed FOXM-immunostaining in the cells expressing Rab5 (Q79L), which is a constitutively active Rab5 mutant impairing endosomal trafficking and allows the observation of MVBs feasible[25]. We detected FOXM1 at the membrane of MVBs in GFP-Rab5(Q79L)-expressed cells, and the knockout of Atg5 abolished this localization (**Fig. 3c and Extended Data Fig. 13a**). Furthermore, FOXM1 co-localized with CD63 (an MVB specific marker[26]) in cells (**Extended Data Fig. 13b and c**), same as CD47 (an LC3-associated EV marker[27]) (**Extended Data Fig. 13d and e**). Subsequently, we harvested different fractions from postnuclear supernatants by using a discontinuous sucrose gradient to define MVB compartments[28]. We found that FOXM1 and lipidated LC3-II were enriched in the fractions possessing

Rab7[29], CD63[26] and TSG101[30] (MVB specific markers), but not in the samples from Atg5$^{-/-}$ cells (**Fig. 3d**). We also immunoprecipitated MVBs with CD63 antibody from cell homogenates and confirmed the existence of FOXM1 and lipidated LC3-II in these MVBs, but not in the samples from Atg5$^{-/-}$ cells (**Extended Data Fig. 14a**). Next, we analyzed whether LC3-FOXM1-DNAs were loaded into MVBs. The chromatin DNA could be observed in MVBs of GFP-Rab5(Q79L)-expressed cells (**Extended Data Fig. 14b**). Subsequently, we measured the levels of LC3-M1-ADs in the gradient-harvested or CD63-immunoprecipitated samples and found that LC3-M1-ADs were enriched in MVB-specific compartments, while the knockout of FOXM1 or Atg5 decreased the levels of these DNA in MVBs (**Fig. 3e-g and Extended Data Fig. 14c**), indicating that the LC3-FOXM1-DNA vesicles were transported to cytoplasmic MVBs.

The loading of LC3-FOXM1-DNAs to EVs by FOXM1

It's well known that MVBs generally fuse with plasma membrane to release ILVs that are then called exosomes, a major type of EVs[31]. To confirm that cytoplasmic LC3-FOXM1-DNAs finally existed in EVs, we first tested whether FOXM1 and LC3 proteins were present in EVs with the collected EV samples by serial differential ultracentrifugation, from which the Large EVs (lEVs) were collected at 15,000×g and the Small EVs (sEVs) were collected at 120,000×g, respectively[32] (**Extended Data Fig. 15a**). Due to sEVs were the main objects of concern in previous studies[33,34], we decided to focus on sEVs to carry out follow-up experiments and just named sEVs as EVs in this study, except as specifically mentioned. The collected EVs were characterized in terms of size range (80-250 nm) and morphology via nanoparticle tracking analysis and transmission electron microscopy, respectively (**Extended Data Fig. 15b and c**), and then validated by immunoblotting with the EV markers (TSG101[35], CD47[36]) (**Extended Data Fig. 15d**). Consistent with previous findings[6,32], the lipidated

LC3-II was detected in the collected EVs (**Fig. 4a and Extended Data Fig. 15d**). FOXM1 was also present in EVs and showed a higher abundance in sEVs than in lEVs (**Fig. 4a and Extended Data Fig. 16a**). Direct Immunoaffinity Capture (DIC) approach, designed to purify the specific EVs containing a certain protein[24], was able to purify the FOXM1-specific EVs from A549 cells, the GFP-FOXM1-specific EVs from GFP-FOXM1-expressed HEK293T cells, or the GFP-LC3-specific EVs from GFP-LC3-expressed HEK293T cells (**Extended Data Fig. 16b-d**), further proving that both FOXM1 and LC3 were present in EVs. We extracted evDNA from EVs and performed the vertical agarose gel electrophoresis to show a specific pattern of bands (**Fig. 4b and Extended Data Fig. 17a**). Furthermore, a flow cytometer (CytoFLEX, Beckman) was used to detect evDNA at the single-EV level, showing that the population of DNA positive EVs varies from 5%-30% (**Extended Data Fig. 17b and c**), consistent with the previous studies[37]. Next, we performed the sequencing analysis to obtain evDNA sequences (named as EV-ADs) and to identify the overlaps (named as LC3-M1-EV-ADs, n=18) between EV-ADs and LC3-M1-ADs (**Fig. 4c, d and Extended Data Fig. 18a, and Table S2**). We chose five LC3-M1-EV-ADs (LC3-M1-EV-AD1, LC3-M1-EV-AD2, LC3-M1-EV-AD3, LC3-M1-EV-AD4, and LC3-M1-EV-AD5) as examples for following experiments.

It's known that inhibiting the autolysosomal process in cells enhances the fusion between autophagosomes and endosomes to secret cellular cargos[22]. Thus, we tested the effects of chloroquine (CQ), an autolysosome inhibitor[38], on the loading of LC3-FOXM1-DNAs to EVs and observed an elevation of LC3-M1-EV-ADs in the EVs of CQ-treated cells (**Fig. 4e**). To further confirm that LC3-FOXM1-EV-ADs were derived from MVB transport process, we used a chemical compound GW4869 (a specific inhibitor of neutral sphingomyelinase inhibiting EVs secretion[25]) to treat cells and found that it inhibited the loading of FOXM1 protein to EVs (**Extended Data Fig. 18b**) and

consequently reduced the levels of LC3-M1-EV-ADs in the EVs (**Fig. 4f**). These data suggested that the cytoplasmic LC3-FOXM1-DNAs were loaded to EVs through the autophagosome-MVB transport process.

To confirm the roles of FOXM1 on the loading of LC3-FOXM1-DNAs to EVs, we purified evDNA from the EVs of GFP-FOXM1-stable expressing HEK293T cells and showed that the elevation of FOXM1 increased the levels of LC3-M1-EV-ADs in the EVs (**Fig. 4g**). We also extracted evDNA of from the EVs of FOXM1$^{-/-}$ cells and showed that the knockout of FOXM1 decreased the levels of LC3-M1-EV-ADs in the EVs (**Fig. 4h**). As expected, the knockdown of FOXM1 had the similar effects to the levels of LC3-M1-EV-ADs in the EVs (**Extended Data Fig. 18c**). Again, the FOXM1-specific EVs collected through the DIC approach showed an enrichment of LC3-M1-EV-ADs (**Fig. 4i, Extended Data Fig. 18d**). EVs were treated with formaldehyde to cross-link evDNA and proteins, then IP with the antibody specific to FOXM1. The levels of LC3-M1-EV-ADs in the anti-FOXM1-IP evDNA samples were significantly elevated (**Fig. 4j and Extended Data Fig. 18e**), further supporting that FOXM1 mediated the loading of these DNA fragments to EVs. Next, we constructed a plasmid that contained 72x FOXM1 binding sites (p72xM1-binding), which could be bound by recombinant FOXM1 *in vitro* or FOXM1-DBD-GFP protein *in vivo* when transfected into cells (**Extended Data Fig. 19a-c**). We transfected p72xM1-binding or control plasmid at the equal amount into cells and isolated evDNA. The qPCR showed that the DNA of p72xM1-binding appeared more than that of control in EVs (**Fig. 4k**). We also transfected p72xM1-binding into FOXM1$^{-/-}$ or Atg5$^{-/-}$ cells and the levels of p72xM1-binding DNA were dramatically lower in the EVs from these cells than that from WT cells (**Fig. 4l**). These data further confirmed that FOXM1-binding DNAs were loaded to EVs by FOXM1. In addition, we performed a series of experiments to prove that the loading of LC3-FOXM1-DNAs to

EVs relied on the mechanisms of FOXM1-LC3 interaction and LC3 lipidation **(Extended Data Fig. 20a-g)**.

The potential fate of LC3-FOXM1-DNAs of EVs

Recent studies have found that evDNAs mainly localize on outside the lumen of EVs[37]. To determine that LC3-FOXM1-EV-DNAs existed on outside the lumen of EVs, we treated EVs with DNase I and observed the decreased levels of LC3-M1-EV-ADs from the samples of DNase I-treated EVs (**Extended Data Fig. 21a, b**). Furthermore, we treated EVs with the Plasmid-Safe ATP-dependent DNase (PS), which can only digest linear DNA[39], and also observed the decreased levels of LC3-M1-EV-ADs from the samples of PS-treated EVs (**Fig. 5a**), suggesting that LC3-FOXM1-DNAs existed as linear DNA on EVs. This finding was further supported by the results of a newly established assay[40], in which terminal deoxynucleotidyl transferase (Tdt) was used to elongate linear DNAs outside of EVs with poly d(A) and then Oligo d(T) beads were used to capture the linear DNA samples (**Extended Data Fig. 21c**). The increased levels of LC3-M1-EV-ADs were observed in this assay (**Fig. 5b**), further suggesting that LC3-FOXM1-DNAs were linear and mainly existed on the outer membrane of EVs.

To explore the outcome of evDNA, we first tested whether the EVs of parent cells could be absorbed by other cells. First, the collected EVs were labeled with the red fluorescent DiI dye (a membrane-lipophilic chemical[41]) and incubated with A549 cells. The DiI dye alone could only stain the cellular membrane without entering cells (**Extended Data Fig. 22a**) while the red fluorescent dots were detected in cytoplasm of the cells treated with the DiI-labeled EVs (**Fig. 5c and Extended Data Fig. 22b**), demonstrating the absorption of EVs by the cells. Then, the DIC-collected GFP-FOXM1-specific EVs were incubated with A549 cells, and the cell samples were immune-stained

with anti-GFP antibody and imaged to show the absorption of the EVs' GFP-FOXM1 proteins by the cells (**Fig. 5d**). Interestingly, we detected the DAPI-stained DNA signals, which were co-localized with GFP-FOXM1 proteins, in the cells treated with the GFP-FOXM1-specific EVs, implicating that LC3-M1-EV-ADs were also absorbed by the cells (**Fig. 5e**). To make sure the absorption of the LC3-M1-EV-ADs by recipient cells, we selected insect *Spodoptera frugiperda* SF-9 cells as the recipient cells for human cell EVs because it's easy to distinguish human DNA from insect genome sequences. SF-9 cells were incubated with the EVs of human A549 cells and the DNA samples of SF-9 cells were prepared one or three days later. PCR confirmed that LC3-M1-EV-ADs were absorbed by SF-9 cells (**Fig. 5f**). In order to track the end of LC3-M1-EV-ADs in the recipient cells, we cultured the human EVs-treated SF-9 cells for a long period according to the regular cell culture procedure, and then extracted the nuclear DNA from the cells at Week 1 or Week 4 post the EV treatment. Surprisingly, human LC3-M1-EV-ADs could be detected by PCR analyses in the nuclear DNA samples of the SF-9 cells even after 4 weeks of the EV treatment (**Fig. 5g**), implicating that these evDNA might exist stably in the recipient cells.

Discussion

In this study, we have discovered that transcription factor FOXM1 mediates the loading of specific chromatin DNA fragments to EVs. Specifically, certain chromatin DNA fragments are specified by FOXM1 and form LC3-FOXM1-DNA vesicles in cytoplasm. Then the cytoplasmic LC3-FOXM1-DNAs are released in EVs through the process of an autophagosome-MVB transport, providing an example of the transcription factor determining the sources of evDNA from chromatin DNA (**Fig. 5h**). EVs are a heterogeneous group of cell-derived membranous structures containing DNAs, RNAs, proteins, and lipids[24], which are now considered as an additional mechanism for

intercellular communication, allowing cells to exchange genetic materials, proteins, and lipids[31]. Although the biological functions of evDNA are not as deeply explored as that of RNAs and proteins in EVs, the diagnostic value of evDNA has been extensively assessed for multiple diseases[1,2]. There is reason to believe that clarifying the sources of evDNA will help improve its more reliable diagnostic applications. FOXM1 can theoretically specify its binding regions in chromatin directly through its DNA-binding consensus sequence[42] or indirectly through interacting with other transcription factors such as B-Myb, MuvB, and NFY[43], providing a clue to determine the sources of evDNA from certain chromatin DNA loci. Based on this understanding, the accuracy and specificity of disease diagnosis can be improved in the future by focusing on specific sequences in evDNA sequencing data. In addition, the further enrichment analysis of the specific sequences of evDNA can predict certain proteins bound to the sequences, so as to help us to establish the association between the proteins and diseases and deduce the course or progression of the diseases.

The specificity of the sources of evDNA from chromatin DNA also implicates that evDNA plays a role to transmit specific genetic information between cells. In this study, we have found that the certain chromatin DNA fragments of human A549 cells can be detected in the nuclear DNA samples of insect *Spodoptera frugiperda* SF-9 cells treated with the A549-derieved EVs after four weeks, providing an example that evDNA mediates the exchange of genetic information among different cells. Imagining that evDNA-containing EVs of certain cells are able to enter the circulatory system and travel far, we have reason to believe that evDNA may possess important biological roles in exchanging genetic information among tissues. This is an attractive hypothesis that needs to be further studied. In addition, the presence of cytoplasmic DNA can drive cell-autonomous responses such as innate immune activation[44], implicating that evDNA may mediate inflammation of recipient cells. Furthermore, certain

extrachromosomal chromatin particles containing extrachromosomal DNA (ecDNA) and RNA Polymerase II have been identified recently to act as mobile transcriptional enhancers to amplify the genome-wide gene transcription in cancer cells[45,46]. In this study, we notice that FOXM1 and the FOXM1-bound evDNA co-exist in EVs of donor cells and are released together from the EVs into recipient cells through mechanisms as yet unknown. Thus we speculate that evDNA-FOXM1 particles formed by FOXM1 and the FOXM1-bound evDNA may function as mobile enhancers in recipient cells through the similar mechanisms of extrachromosomal chromatin particles.

Although this study focuses on FOXM1 as an example to show that transcription factors determine the sources of evDNA from certain chromatin DNA regions, we anticipate that the FOXM1-LC3 interaction is not an isolated event in nucleus and many other transcription factors can act similarly. We have found that other Forkhead Box transcription factors such as FOXA2 and FOXP2 can interact with LC3 (**Extended Data Fig. 23**), implicating that these two transcription factors may also participate in determining the sources of evDNA from chromatin DNA. In addition, LC3 interacts with multiple transcription factors and EVs contain many transcription factors, both identified by mass spectrometry analysis[6,32], suggesting that these transcription factors may also play a similar role as FOXM1 for specifying evDNA from chromatin DNA. Transcription factors are generally considered to bind to specific DNA regions of chromosome and regulate specific gene expression in nucleus[47]. Based on the fact that FOXM1 interacts with LC3 to determine the sources of evDNA, the findings of this study expand the understanding of the functions of transcription factors and provide a new perspective to explore their roles in regulating the composition of EVs' DNA components.

FOXM1 is involved in regulating cell proliferation[48], DNA damage repair[49], cell stemness[50], and metastasis[51,52] through stimulating gene transcription in nucleus[7]. The further research on the

association among FOXM1, evDNA, and EVs may update the understanding of how FOXM1 performs its various functions. More importantly, one key question that still remains to be answered is how chromatin DNA breaks to generate specific fragments. So far, the formation of chromatin DNA in cytoplasm is considered mainly through the micronuclei and cytoplasmic chromatin fragment pathways[44], but both cannot determine the specificity of chromatin DNA breakage. Although LC3 is found to interact with nuclear LaminB1 protein in nucleus and result in the cytoplasmic translocation of transcriptionally inactive heterochromatin DNA[5], the mechanism by which specific DNA fragments break off chromosomes has not been explored. Recently, the complex of Rec114, Mei4 and Mer2 in yeast has been reported to execute and control DNA breakage[53], suggesting that the breakage of specific chromatin DNA can be precisely achieved. Future studies of FOXM1's interaction with the controlled DNA breakage machinery will help reveal how relevant chromatin DNA fragments are produced. On the other hand, although there is no evidence so far, certain chromatin DNA fragments produced by FOXM1-LC3 may act as ecDNA directly in nucleus. Therefore, investigating FOXM1-LC3-mediated specific chromatin DNA breakage in the future will not only help to clarify the sources of evDNA but also provide clues to answer whether certain transcription factors such as FOXM1 are involved in the ecDNA generation.

Materials and Methods

The complete Materials and Methods were described in Supplementary Materials.

ChIP sequencing, evDNA sequencing, Bioinformatics analysis, RT-qPCR. For sequencing, ChIP and evDNA samples were prepared as described previously[54]. The ChIP and evDNA were then purified and used for constructing sequencing libraries with a NEBNext Ultra DNA Library Prep Kit for Illumina (New England Biolabs, Ipswich, MA, USA). The library quantifications were assessed on the Agilent Bioanalyzer 2100 system. The library preparations were sequenced on an Illumina Hiseq platform and 50 bp single-end reads or 150 bp paired-end reads were generated.

For bioinformatics analysis, the following pipeline was used for analysis of all sequence data sets. Firstly, fastp (version 0.20.0, parameter: '-q 15 -u 40 -n 6 -l 15 ')[55] was used to trim adaptors and low-quality reads. Then, we evaluated the quality of NGS short reads by searching them on the FastQC (version 0.11.8) program (http://www.bioinformatics.babraham.ac.uk/projects/fastqc). Thirdly, the remaining reads were aligned to human genome hg38 by bwa men (version 0.7.17,parameter: '-t 20')[56], since ChIP-Seq and evDNA-Seq interrupted fragments were usually small and the percentage of unique sequences in the total number of sequences was the focus of attention. Finally, peak calling of the aligned reads was made using macs3 (version 3.0.0a6, parameter: '-f BAM -g hs -p 0.1 -B')[57], and peaks were annotated using the R/Bioconductor package ChIPseeker[58]. Browser views of peaks are shown using Integrated Genomics Viewer (IGV; broadinstitute.org/igv)[59].

For RT-qPCR, the following primers were used for qPCR analyses of LC3-M1-ADs. LC3-M1-AD1 (chr12): forward, 5'-CCA CTT TGA TGG GTC TCG CT-3'; reverse, 5'-TGT CTG GTG ACC GTT GGT TC-3'. LC3-M1-AD2 (chr12): forward, 5'-GAT GGT GTG TGG CTG TAA CAT-3'; reverse, 5'-CTG TGG CCG TGT AAG GCT AT-3'. LC3-M1-AD3 (chr10): forward, 5'-GGG

ATA TGT GAA AAC GCC CC-3'; reverse, 5'-CTG CCT ACA GGG AAT TTC GA-3'.

The following primers were used for qPCR analyses of LC3-M1-EV-ADs. LC3-M1-EV-AD1 (chr12) is the same as LC3-M1-AD1; LC3-M1-EV-AD2 (chr10) is the same as LC3-M1-AD3; LC3-M1-EV-AD3 (chr8): forward, 5'-GTT TTC ACA GCC ACT GCA GG-3'; reverse, 5'-ACT CCC GTC AGA GCA ACA TG-3'. LC3-M1-EV-AD4 (chr4): forward, 5'-TCA CAA GCC CCC TGT AGG-3'; reverse, 5'-TCC AAC TCT TGC CTG GTC TC-3'. LC3-M1-EV-AD5 (chr5): forward, 5'-TTC ACG TTT CCC TCA CCC AG-3'; reverse, 5'-TGA GAC ATT TTA CGA AGT TGA GCA-3'.

DNA Fluorescence *in situ* hybridization (FISH). DNA-FISH probes were constructed by Exon Biotechnology Inc (Guangzhou, China). The probes covered genomic regions (hg19) used in this study is as follow: chr12: 2853923-2864350 (hg19_ LC3-M1-AD1_10 Kb).

For fluorescence *in situ* hybridization assay, DNA FISH was performed as described[60]. Briefly, coverslips containing fixed and permeabilized cells were quenched by 3% H_2O_2, followed by dehydration in 70%, 85%, and 100% ethanol for 1 min each. FISH probe (hg19_ LC3-M1-AD1_10 Kb) was added onto a glass slide, and lower the coverslips onto the slide slowly. Place the slides with samples to be hybridized in a heating block at 85℃ for 5min, and then 37℃ for 20 hours. The slide was then removed, and the sample was washed with Wash Buffer (1 X, preheated to 73℃) for 2 min. Added blocking buffer onto the hybridized samples and incubated at 37℃ for 30 min. Added primary antibody onto coverslip and incubated at 37℃ for 30 min. The sample was washed with Wash Buffer (1 X, preheated to 45℃) for 5 min. Added secondary antibody onto coverslip and incubated at 37℃ for 30 min. Wash coverslip in Wash Buffer (1x) three times at 45℃ for 5 min. Re-wash once with PBS. Preparation of TSA solution at TSA: 0.15%H2O2: TSA amplification buffer = 1:5:500-1:10:1000. Add TSA solution to coverslip and incubate 5-15min at RT. Wash coverslip in Wash Buffer (1 X) three

times for 30 min. Mount coverslip with Anti-fade Fluorescence Mounting Medium (with DAPI, Abcam, #ab104139).

CRISPR/Cas9-mediated knock-in of a TetO array (96x) for visualization of LC3-M1-AD3 loci. To obtain a TetO-knockin cell line, we designed a pair of gRNAs using http://crispr.mit.edu/. The pair of gRNAs (5'-CAC CTG GGT GAT CAG AGC AA-3' and 5'-TCT AGG CTT TGG CCT ACA GG-3') bound to LC3-M1-AD3 loci and were cloned into the pX335 vector (Addgene, 42335) before the gRNA scaffold. Furthermore, we designed a donor so that the plasmid DNA contains the TetO array (96x) flanked by 500-bp homology arms of the LC3-M1-AD3. The primers: 5'-CCC TTT CGT CTT CAA GAA TTC CAT CAC CTG GGT GAT CAG TGT AGA-3', 5'-ACC CAT TCC TAG GGC GAA TTC GCT CTC TGA TCA CCC AGG TGA T-3'; 5'-GCG CTGC TAG CTT AAG GTA CCA GCG TAG GCC AAA GCC TAG AC-3', 5'-CCC AGA TCT ATC GAT GGT ACC CTT GTC TAG GAT CTG CCT ACA GGG-3' were synthesized and amplified homology arms of the LC3-M1-AD3 to clone into the pSP2-96-merTetO-EFS-BLaR vector (Addgene, 118713). The paired gRNAs and donor plasmids were co-transfected into A549 cells. Blasticidin (10 μg/ml) selection was started 1 day after transfection. Three weeks after blasticidin selection, TetO-knockin cell clones were transplanted into 24-well plates. Cells were collected from 24-well plates and extracted genomic DNA (gDNA) for genotyping.

For LC3-M1-AD3 loci visualization, the TetO-knockin cells were transfected with TetR-GFP plasmid. After 48 hours, cells were fixed in 4% paraformaldehyde and mounted with Mounting Medium with DAPI (Abcam, ab104139). Images were captured by FV1200 laser scanning microscopes (Olympus, Japan).

Extracellular vesicle isolation. Cells seeded in 150 mm culture dishes at approximately 80%

confluence were incubated with serum-free DMEM for 1 day or 3 days. Cell viability was assessed using trypan blue and only > 95% viability was used for EVs isolation. The cell-conditioned medium was collected by sequential ultracentrifugation[6,24]. Briefly, the medium was first subjected to a centrifugation at 400 × g for 10 min to remove cells. Next, the supernatant was centrifuged at 2,000 × g for 20 min to remove debris and apoptotic bodies. Then, the supernatant was centrifuged at 15,000 × g for 40 min to obtain large EVs. The resulting large EVs pellet was resuspended in a large volume of PBS buffer followed by ultracentrifugation at 15,000 × g for 40 min to wash the sample. To remove any remaining any large EVs, the media supernatant from the first 15,000 × g step was passed through a 0.22-μm pore PES filter (Millipore, Bedford, MA, USA). This supernatant (pre-cleared medium) was next subjected to ultracentrifugation at 120,000 × g for 4 h in a SW 28 Ti Swinging-Bucket Rotor (Beckman Coulter, Fullerton, CA) to sediment small EVs. The crude small EVs pellet was resuspended in a large volume of PBS followed by ultracentrifugation at 120,000 × g for 4 h to wash the sample. All following centrifugation steps were performed at 4℃. Notably, for the comparison of EVs in different conditions, the results must be corrected by total cell number or total protein concentration to eliminate differences in cell seeding.

Acknowledgements

We thank Dr. Zhuoxian Rong of Central South University for help with construction of FOXM1 knockout HEK293T cell line by CRISPR/Cas9 technology; thank Dr. Feng Yu of Hunan University for sharing SF-9 cell line; thank Dr. Jianhui Jiang of Hunan University for help with confocal microscopy. This work was supported by the National Natural Science Foundation of China (grant number 81773169 to Y.T.), China Changsha Development and Reform Commission "Mass entrepreneurship and innovation program" (2018-68) and "Innovation platform construction program" (2018-216).

Author contributions

Y.Z. and Y.T. conceived this project. Y.Z., N.D., Y.L., X.Z., S.Y., R.W., H.L. and Y.W. performed all of experiments. Y.Z., H.C., P.F., Y.P., L.Y. and T.Y. analyzed ChIP-seq and evDNA-seq. M.O. performed molecular docking simulation. Y.C, L.Y. and X.H. provided administrative and material supports. Y.T. supervised this study. Y.Z. and Y.T. composed the manuscript. All authors reviewed the manuscript and discussed the work.

Competing interests

The authors declare no competing interests.

Supplementary Material

Supplementary methods, figures and tables.

References

1 Sina, A. A. *et al.* Methylation dependent gold adsorption behaviour identifies cancer derived extracellular vesicular DNA. *Nanoscale Horiz* **5**, 1317-1323 (2020).

2 Elzanowska, J., Semira, C. & Costa-Silva, B. DNA in extracellular vesicles: biological and clinical aspects. *Mol Oncol* **15**, 1701-1714 (2020).

3 Wierstra, I. & Alves, J. FOXM1, a typical proliferation-associated transcription factor. *Biol Chem* **388**, 1257-1274 (2007).

4 Lee, Y. K. & Lee, J. A. Role of the mammalian ATG8/LC3 family in autophagy: differential and compensatory roles in the spatiotemporal regulation of autophagy. *BMB Rep* **49**, 424-430 (2016).

5 Dou, Z. *et al.* Autophagy mediates degradation of nuclear lamina. *Nature* **527**, 105-109 (2015).

6 Leidal, A. M. *et al.* The LC3-conjugation machinery specifies the loading of RNA-binding proteins into extracellular vesicles. *Nat Cell Biol* **22**, 187-199 (2020).

7 Sanders, D. A. *et al.* FOXM1 binds directly to non-consensus sequences in the human genome. *Genome Biol* **16**, 130 (2015).

8 Tasan, I. *et al.* CRISPR/Cas9-mediated knock-in of an optimized TetO repeat for live cell imaging of endogenous loci. **46**, e100 (2018).

9 Abmayr, S. M., Yao, T., Parmely, T. & Workman, J. L. Preparation of nuclear and cytoplasmic extracts from mammalian cells. *Curr Protoc Mol Biol* **Chapter 12**, Unit 12 11 (2006).

10 Tanida, I., Ueno, T. & Kominami, E. LC3 conjugation system in mammalian autophagy. *Int J Biochem Cell Biol* **36**, 2503-2518 (2004).

11 Hu, C. D. & Kerppola, T. K. Simultaneous visualization of multiple protein interactions in living cells using multicolor fluorescence complementation analysis. *Nat Biotechnol* **21**, 539-545 (2003).

12 Birgisdottir, A. B., Lamark, T. & Johansen, T. The LIR motif - crucial for selective autophagy. *J Cell Sci* **126**, 3237-3247 (2013).

13 Johansen, T. & Lamark, T. Selective Autophagy: ATG8 Family Proteins, LIR Motifs and Cargo Receptors. *J Mol Biol* **432**, 80-103 (2020).

14 Barlow, K. A. *et al.* Flex ddG: Rosetta Ensemble-Based Estimation of Changes in Protein-Protein Binding Affinity upon Mutation. *J Phys Chem B* **122**, 5389-5399 (2018).

15 Kuang, Y. *et al.* Structural basis for the phosphorylation of FUNDC1 LIR as a molecular switch of mitophagy. *Autophagy* **12**, 2363-2373 (2016).

16 Sentelle, R. D. *et al.* Ceramide targets autophagosomes to mitochondria and induces lethal mitophagy. *Nat Chem Biol* **8**, 831-838 (2012).

17 Chaudhury, S. *et al.* Benchmarking and analysis of protein docking performance in Rosetta v3.2. *PLoS One* **6**, e22477 (2011).

18 Littler, D. R. *et al.* Structure of the FoxM1 DNA-recognition domain bound to a promoter sequence. *Nucleic Acids Res* **38**, 4527-4538 (2010).

19 Otomo, C., Metlagel, Z., Takaesu, G. & Otomo, T. Structure of the human ATG12~ATG5 conjugate required for LC3 lipidation in autophagy. *Nat Struct Mol Biol* **20**, 59-66 (2013).

20 Itakura, E., Kishi-Itakura, C. & Mizushima, N. The hairpin-type tail-anchored SNARE syntaxin 17 targets to autophagosomes for fusion with endosomes/lysosomes. *Cell* **151**, 1256-1269

452 (2012).
453 21 Diao, J. *et al.* ATG14 promotes membrane tethering and fusion of autophagosomes to
454 endolysosomes. *Nature* **520**, 563-566 (2015).
455 22 Fader, C. M. & Colombo, M. I. Autophagy and multivesicular bodies: two closely related
456 partners. *Cell Death Differ* **16**, 70-78 (2009).
457 23 Leidal, A. M. & Debnath, J. Emerging roles for the autophagy machinery in extracellular
458 vesicle biogenesis and secretion. *FASEB Bioadv* **3**, 377-386 (2021).
459 24 Jeppesen, D. K. *et al.* Reassessment of Exosome Composition. *Cell* **177**, 428-445 e418 (2019).
460 25 Trajkovic, K. *et al.* Ceramide triggers budding of exosome vesicles into multivesicular
461 endosomes. *Science* **319**, 1244-1247 (2008).
462 26 Piper, R. C. & Katzmann, D. J. Biogenesis and function of multivesicular bodies. *Annu Rev Cell*
463 *Dev Biol* **23**, 519-547 (2007).
464 27 Wang, H. S., Pei, F., Chen, Z. & Zhang, L. Increased Apoptosis of Inflamed Odontoblasts Is
465 Associated with CD47 Loss. *J Dent Res* **95**, 697-703 (2016).
466 28 de Araujo, M. E., Lamberti, G. & Huber, L. A. Homogenization of Mammalian Cells. *Cold Spring*
467 *Harb Protoc* **2015**, 1009-1012 (2015).
468 29 Shearer, L. J. & Petersen, N. O. Distribution and Co-localization of endosome markers in cells.
469 *Heliyon* **5**, e02375 (2019).
470 30 Nabhan, J. F., Hu, R., Oh, R. S., Cohen, S. N. & Lu, Q. Formation and release of arrestin
471 domain-containing protein 1-mediated microvesicles (ARMMs) at plasma membrane by
472 recruitment of TSG101 protein. *Proc Natl Acad Sci U S A* **109**, 4146-4151 (2012).
473 31 van Niel, G., D'Angelo, G. & Raposo, G. Shedding light on the cell biology of extracellular
474 vesicles. *Nat Rev Mol Cell Biol* **19**, 213-228 (2018).
475 32 Hoshino, A. *et al.* Extracellular Vesicle and Particle Biomarkers Define Multiple Human
476 Cancers. *Cell* **182**, 1044-1061 e1018 (2020).
477 33 Moller, A. & Lobb, R. J. The evolving translational potential of small extracellular vesicles in
478 cancer. *Nat Rev Cancer* **20**, 697-709 (2020).
479 34 Gao, Y. *et al.* Small Extracellular Vesicles: A Novel Avenue for Cancer Management. *Front*
480 *Oncol* **11**, 638357 (2021).
481 35 Yoshioka, Y. *et al.* Comparative marker analysis of extracellular vesicles in different human
482 cancer types. *J Extracell Vesicles* **2**, eCollection 2013 (2013).
483 36 Kaur, S. *et al.* CD63, MHC class 1, and CD47 identify subsets of extracellular vesicles
484 containing distinct populations of noncoding RNAs. *Sci Rep* **8**, 2577 (2018).
485 37 Liu, H. *et al.* Analysis of extracellular vesicle DNA at the single-vesicle level by nano-flow
486 cytometry. *J Extracell Vesicles* **11**, e12206 (2022).
487 38 Mauthe, M. *et al.* Chloroquine inhibits autophagic flux by decreasing
488 autophagosome-lysosome fusion. *Autophagy* **14**, 1435-1455 (2018).
489 39 Wang, Y. *et al.* eccDNAs are apoptotic products with high innate immunostimulatory activity.
490 *Nature* **599**, 308-314 (2021).
491 40 Fan, W. *et al.* Nucleic Acid Substrate-Independent DNA Polymerization on the Exosome
492 Membrane: A Mechanism Study and Application in Exosome Analysis. *Anal Chem* **94**,
493 2172-2179 (2022).
494 41 Yektaeian, N. *et al.* Lipophilic tracer Dil and fluorescence labeling of acridine orange used for
495 Leishmania major tracing in the fibroblast cells. *Heliyon* **5**, e03073 (2019).

496 42 Marceau, A. H. *et al.* An order-to-disorder structural switch activates the FoxM1 transcription
497 factor. *Elife* **8**, e46131 (2019).
498 43 Liu, C., Barger, C. J. & Karpf, A. R. FOXM1: A Multifunctional Oncoprotein and Emerging
499 Therapeutic Target in Ovarian Cancer. *Cancers (Basel)* **13**2021).
500 44 Miller, K. N. *et al.* Cytoplasmic DNA: sources, sensing, and role in aging and disease. *Cell* **184**,
501 5506-5526 (2021).
502 45 Zhu, Y. *et al.* Oncogenic extrachromosomal DNA functions as mobile enhancers to globally
503 amplify chromosomal transcription. *Cancer Cell* **39**, 694-707 e697 (2021).
504 46 Hung, K. L. *et al.* ecDNA hubs drive cooperative intermolecular oncogene expression. *Nature*
505 **600**, 731-736 (2021).
506 47 Todeschini, A. L., Georges, A. & Veitia, R. A. Transcription factors: specific DNA binding and
507 specific gene regulation. *Trends Genet* **30**, 211-219 (2014).
508 48 Fu, Z. *et al.* Plk1-dependent phosphorylation of FoxM1 regulates a transcriptional programme
509 required for mitotic progression. *Nat Cell Biol* **10**, 1076-1082 (2008).
510 49 Tan, Y., Raychaudhuri, P. & Costa, R. H. Chk2 mediates stabilization of the FoxM1 transcription
511 factor to stimulate expression of DNA repair genes. *Mol Cell Biol* **27**, 1007-1016 (2007).
512 50 Song, I. S. *et al.* FOXM1-Induced PRX3 Regulates Stemness and Survival of Colon Cancer Cells
513 via Maintenance of Mitochondrial Function. *Gastroenterology* **149**, 1006-1016 e1009 (2015).
514 51 Xie, Z. *et al.* Foxm1 transcription factor is required for maintenance of pluripotency of P19
515 embryonal carcinoma cells. *Nucleic Acids Res* **38**, 8027-8038 (2010).
516 52 Li, D. *et al.* The critical role of dysregulated FOXM1-PLAUR signaling in human colon cancer
517 progression and metastasis. *Clin Cancer Res* **19**, 62-72 (2013).
518 53 Claeys Bouuaert, C. *et al.* DNA-driven condensation assembles the meiotic DNA break
519 machinery. *Nature* **592**, 144-149 (2021).
520 54 Kharchenko, P. V., Tolstorukov, M. Y. & Park, P. J. Design and analysis of ChIP-seq experiments
521 for DNA-binding proteins. *Nat Biotechnol* **26**, 1351-1359 (2008).
522 55 Chen, S., Zhou, Y., Chen, Y. & Gu, J. fastp: an ultra-fast all-in-one FASTQ preprocessor.
523 *Bioinformatics* **34**, i884-i890 (2018).
524 56 Li, H. Aligning sequence reads, clone sequences and assembly contigs with BWA-MEM. *arXiv*
525 **1303.3997** (2013).
526 57 Zhang, Y. *et al.* Model-based analysis of ChIP-Seq (MACS). *Genome Biol* **9**, R137 (2008).
527 58 Yu, G., Wang, L. G. & He, Q. Y. ChIPseeker: an R/Bioconductor package for ChIP peak
528 annotation, comparison and visualization. *Bioinformatics* **31**, 2382-2383 (2015).
529 59 Robinson, J. T. *et al.* Integrative genomics viewer. *Nat Biotechnol* **29**, 24-26 (2011).
530 60 Tsuchiya, K. D. Fluorescence in situ hybridization. *Clin Lab Med* **31**, 525-542, vii-viii (2011).
531 61 Collier, J. J. *et al.* Developmental Consequences of Defective ATG7-Mediated Autophagy in
532 Humans. *N Engl J Med* **384**, 2406-2417 (2021).
533

Figures

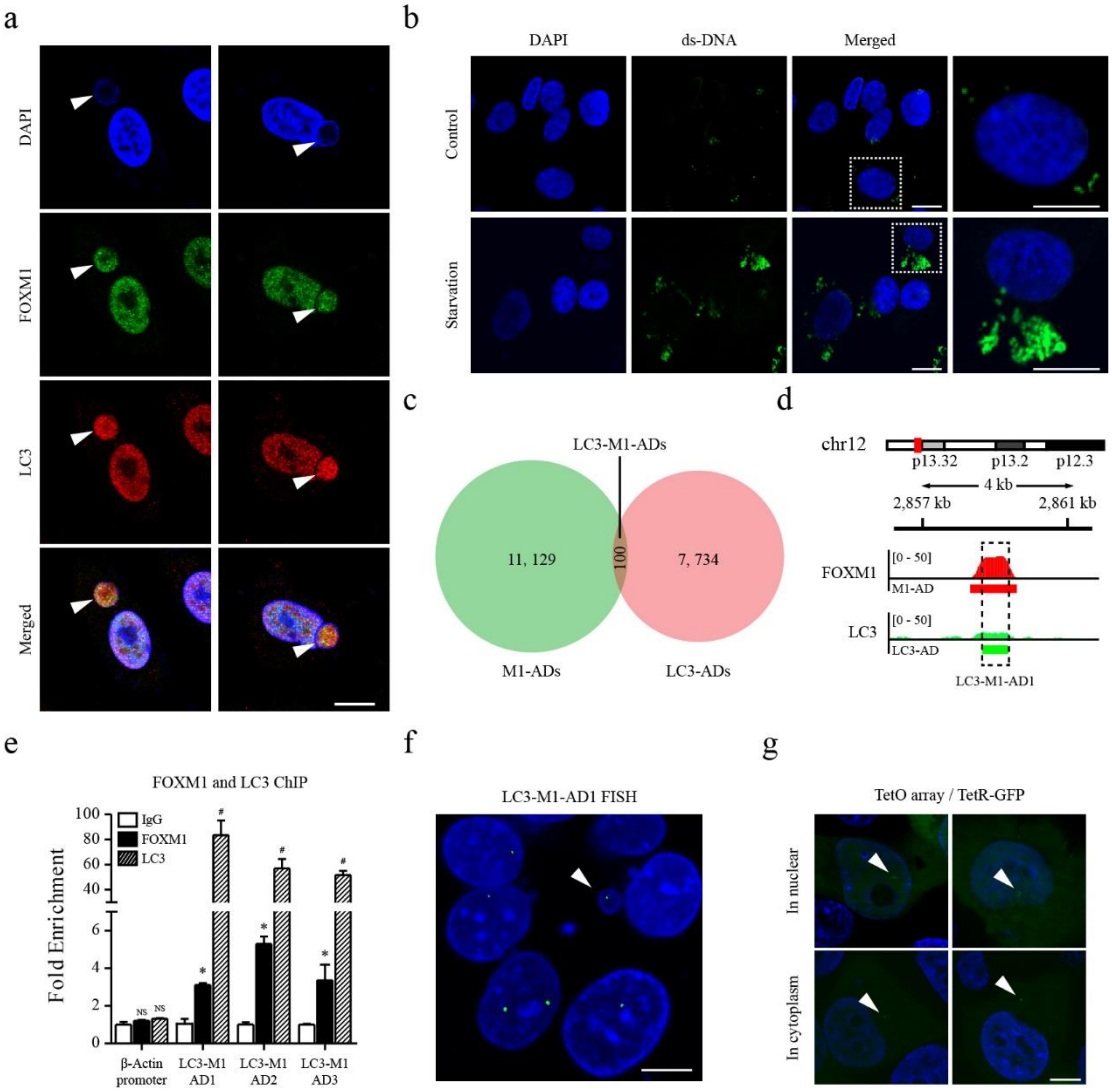

Figure 1. The formation of LC3-FOXM1-DNA vesicles in cytoplasm. (a) The LC3-FOXM1-DNA vesiculation in A549 cells. The white arrows indicate LC3-FOXM1-DNA vesicle. **(b)** The immunofluorescent staining of an anti-dsDNA antibody showed cytoplasmic dsDNA under starvation (6 hrs). **(c)** The overlaps (LC3-M1-ADs, n=100) between M1-ADs (n=11229) and LC3-ADs (n=7834) were identified in genome. **(d)** A representative overlap (LC3-M1-AD1) on chr12 between M1-ADs and LC3-ADs. **(e)** The FOXM1 and LC3 ChIP-qPCR of LC3-M1-ADs in A549 cells. The Bars, mean±s.e.m.; n=3; **P*<0.05, #*P*<0.05; NS, non-significant; unpaired two-tailed. **(f)** Representative DNA-FISH images of LC3-M1-AD1-adjacent region (10 Kb probe) in A549 cells. The white arrows

indicate LC3-M1-AD1. **(g)** Representative TetR-GFP images of TetO array (96x) at the locus of LC3-M1-AD3 in A549 cells. The white arrows indicate TetO array (96x) at the locus of LC3-M1-AD3. Scale bars, 10 μm.

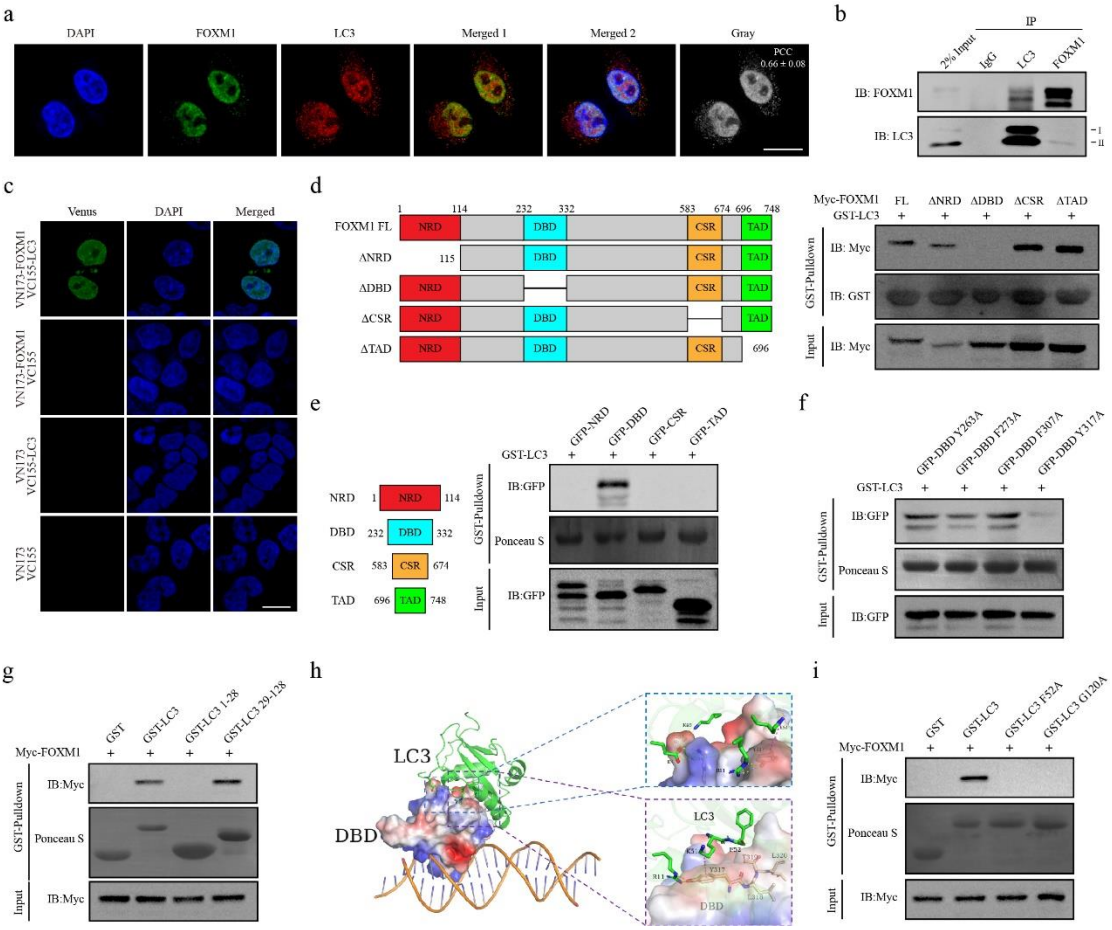

Figure 2. The interaction between FOXM1 and LC3. (a) Immunofluorescence staining of FOXM1 and LC3 in A549 cells. Scale bar, 10 μm. The Pearson Correlation Coefficient (PCC) value of FOXM1 and LC3 colocalization was 0.66±0.08. **(b)** Co-immunoprecipitation of endogenous FOXM1 and LC3 in A549 cells. **(c)** The BiFC assays of FOXM1-LC3 interaction. HEK293T cells were transfected with the indicated combination of split Venus constructs for 24 hrs. Scale bar, 10 μm. **(d)** The Myc-tagged FOXM1 deletion mutants were pulled down with bacterially purified GST-LC3 as indicated. **(e)** The GFP-fused FOXM1 truncations were pulled down with bacterially purified GST-LC3 as indicated. **(f)** The GFP-fused FOXM1-DBD point mutations were pulled down with bacterially purified GST-LC3 as indicated. **(g)** The Myc-tagged FOXM1 was pulled down with bacterially purified GST-LC3 truncated mutants. **(h)** The molecular docking simulation for FOXM1-LC3 interaction by Rosetta Dock. **(i)** The Myc-tagged FOXM1 was pulled down with bacterially purified GST-LC3 point mutated proteins.

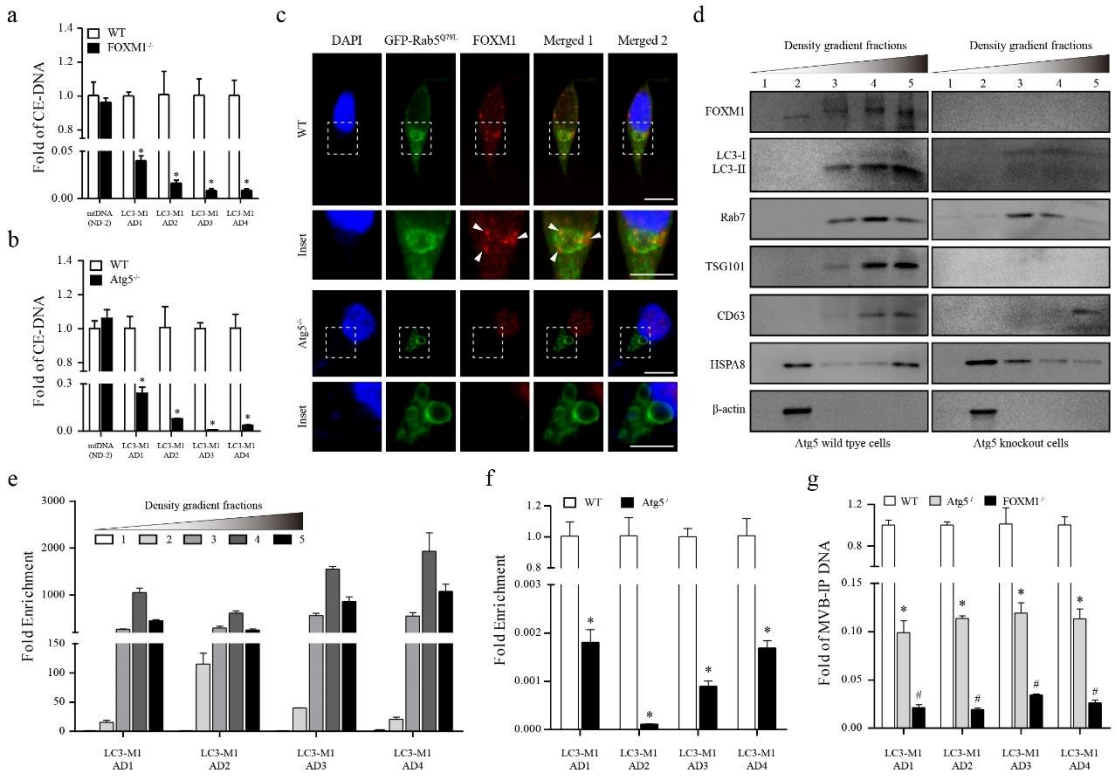

Figure 3. The transport of LC3-FOXM1-DNAs to cytoplasmic MVBs. (a) The cytoplasmic DNA (CE-DNA) was extracted from WT or FOXM1$^{-/-}$ cells for qPCR. **(b)** The cytoplasmic DNA (CE-DNA) was extracted from WT or Atg5$^{-/-}$ cells for qPCR. **(c)** Immunofluorescence using confocal microscopy showed that endogenous FOXM1 localized in GFP-Rab5 (Q79L) compartments in A549 cells. The white arrows indicate the localization of FOXM1 in ILVs. Scale bar, 10 μm. **(d)** MVB compartments were isolated by discontinuous sucrose gradient and subjected to immunoblotting. **(e)** The qPCR analyses of LC3-M1-ADs in ultracentrifuged-MVB fractions from A549 cells. **(f)** The qPCR analyses of LC3-M1-ADs in ultracentrifuged-MVB fractions 4 from WT or Atg5$^{-/-}$ cells. **(g)** The qPCR analyses of LC3-M1-ADs in the CD63-immunoprecipitated MVBs collected from WT, Atg5$^{-/-}$ or FOXM1$^{-/-}$ cells. The Bars, mean±s.e.m.; n=3; *$P < 0.05$; unpaired two-tailed.

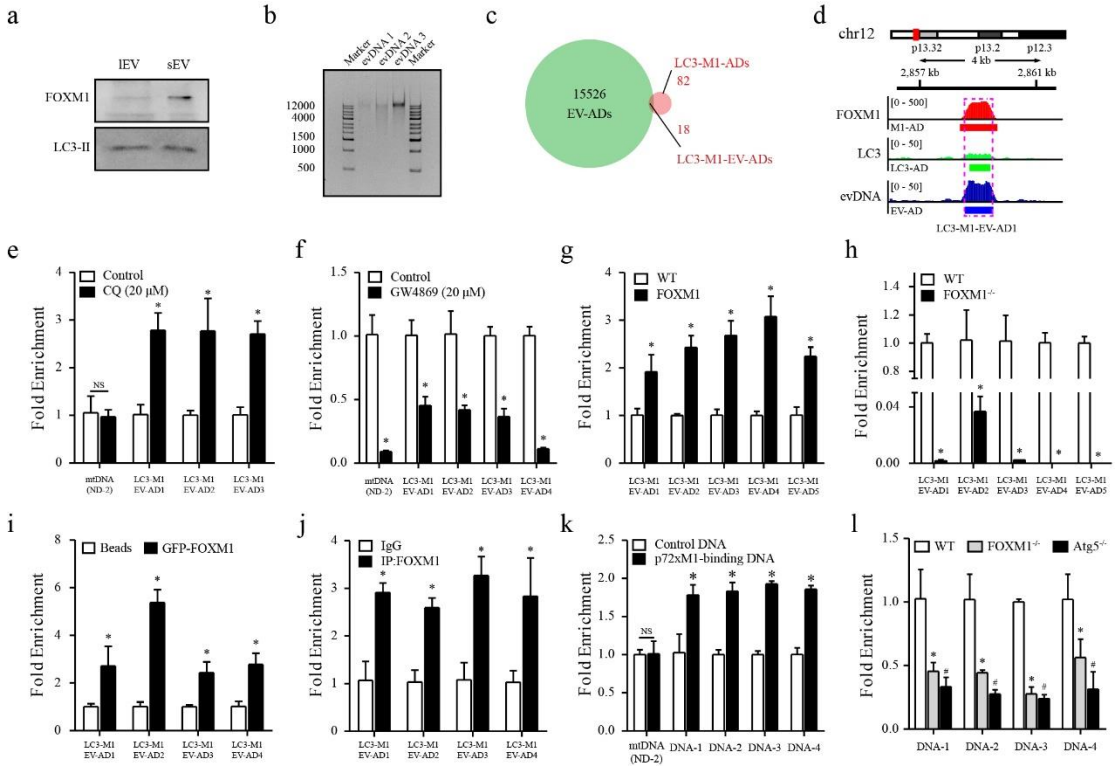

Figure 4. The loading of LC3-FOXM1-DNAs to EVs by FOXM1. (a) A549-derived extracellular vesicles were subjected to immunoblotting. lEV, Large extracellular vesicles; sEV, Small extracellular vesicles. **(b)** The vertical agarose gel showed evDNAs purified from A549 cells, n=3. Shown are representatives of three independent experiments. (**c**) The overlaps (LC3-M1-EV-ADs, n=18) between EV-ADs (n=15544) and LC3-M1-ADs (n=100) were identified. **(d)** A representative overlap (LC3-M1-EV-AD1) on chr12 between EV-ADs and LC3-M1-ADs. **(e)** The qPCR analyses of LC3-M1-EV-ADs in the EVs collected A549 cells that were treated with CQ (20 μM) for 24 hours. **(f)** The qPCR analyses of LC3-M1-EV-ADs in the EVs collected from A549 cells that were treated with GW4869 (20 μM) for 24 hours. **(g)** The qPCR analyses of LC3-M1-EV-ADs in the EVs collected from FOXM1-overexpressing HEK293T cells. **(h)** The qPCR analyses of LC3-M1-EV-ADs in the EVs collected from FOXM1-knockout HEK293T cells by CRISPR-cas9. **(i)** The qPCR analyses of LC3-M1-EV-ADs in the DIC-purified GFP-FOXM1-specific EVs collected from A549 cells. **(j)** The qPCR analyses of LC3-M1-EV-ADs in anti-FOXM1-IP evDNA. **(k)** The qPCR analyses of

p72xM1-binding DNA or control DNA in the EVs collected from HEK293T cells transfected as indicated. **(l)** The qPCR analyses of p72xM1-binding DNA sequences in the EVs collected from WT, FOXM1$^{-/-}$ and Atg5$^{-/-}$ cells. The Bars, mean±s.e.m.; n=3; *P < 0.05; #P<0.05; NS, non-significant; unpaired two-tailed.

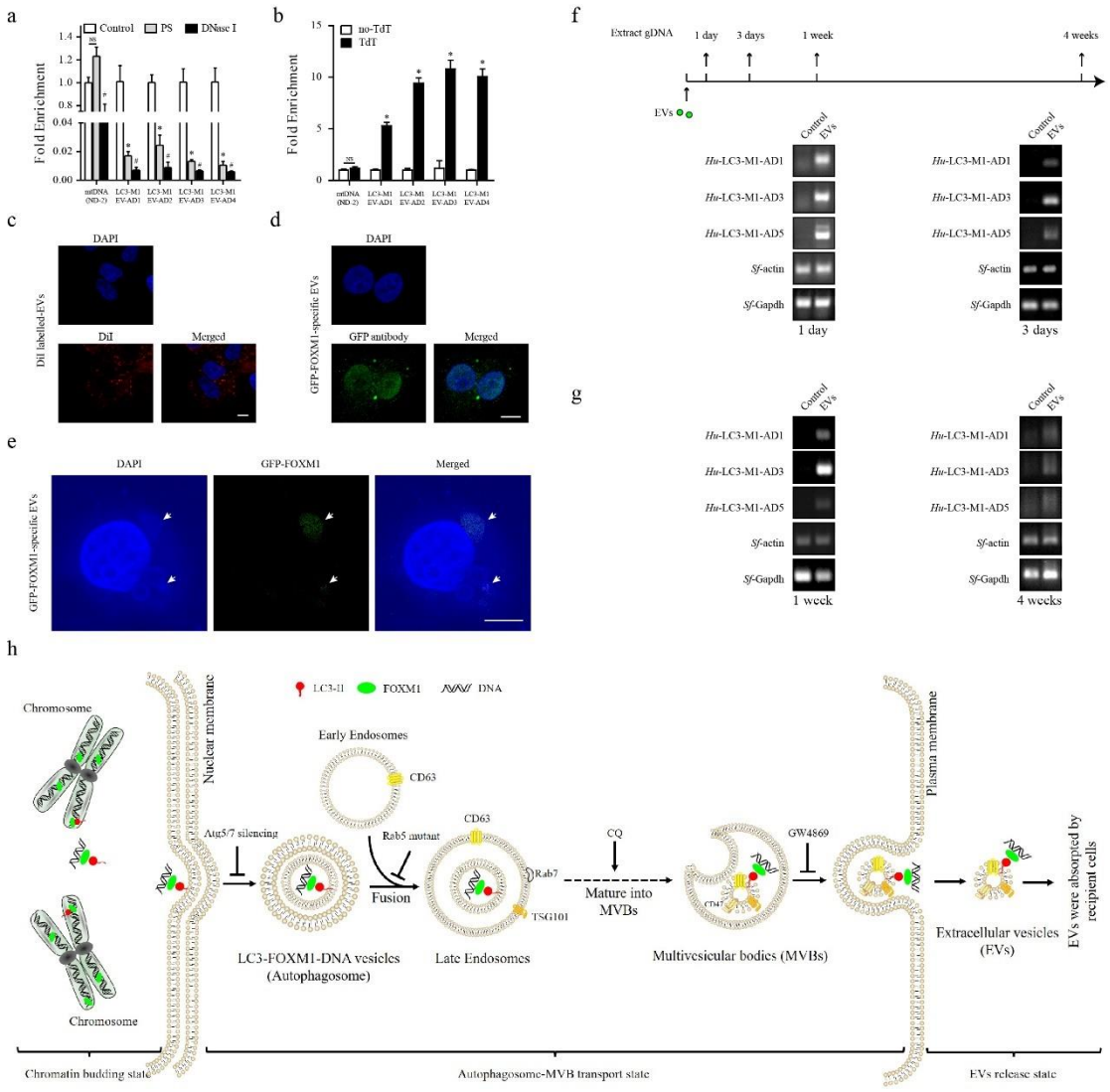

Figure 5. The potential fate of LC3-FOXM1-DNAs of EVs. (a) The qPCR analyses of LC3-M1-EV-ADs in the EVs that were treated with Plasmid-Safe ATP-dependent DNase (PS, digest linear DNA) or DNase I (digest single or double stranded DNA). **(b)** The qPCR analyses of LC3-M1-EV-ADs in the TdT-catalyzed EVs collected from A549 cells. The Bars, mean±s.e.m.; n=3; *P<0.05, #P<0.05; NS, non-significant; unpaired two-tailed. **(c)** Fluorescent imaging of A549 cells incubated 12 hrs with DiI dye-labelled EVs. **(d)** A549 cells were incubated 12 hrs with DIC-purified GFP-FOXM1-specific EVs and immunostained by anti-GFP antibody for fluorescent imaging. **(e)** Fluorescent imaging of A549 cells incubated 12 hrs with DIC-purified GFP-FOXM1-specific EVs. The signals of DAPI were overexposed. Scale bar, 10 μm. **(f)** Insect *Spodoptera frugiperda* SF-9 cells were

treated with human A549 cells-derived EVs and one or three days later the genomic DNA was extracted for PCR analyses of human LC3-M1-EV-ADs. **(g)** SF-9 cells were treated as (f) and one or four weeks later the genomic DNA was extracted for PCR analyses of human LC3-M1-EV-ADs. **(h)** Schematic illustration of evDNA biogenesis. Atg5[19] and Atg7[61], autophagy regulator essential for LC3 lipidation; CD63[26], Rab7[29] and TSG101[30], MVB specific markers; Rab5[29], a early endosome marker; CQ, an autolysosome inhibitor[38]; GW4869, a specific inhibitor of neutral sphingomyelinase and inhibit EVs secretion[25].